RSC Advances

PAPER

View Article Online
View Journal | View Issue

Cite this: *RSC Adv.*, 2023, **13**, 12476

Carbazole fluorophore with an imidazole/thiazole unit: contrasting stimuli-induced fluorescence switching, water-sensing and deep-blue emission†

Sasikala Ravi,[a] P. R. Nithiasri,[a] Subramanian Karthikeyan,[b] Mehboobali Pannipara,[cd] Abdullah G. Al-Sehemi,[cd] Dohyun Moon *[e] and Savarimuthu Philip Anthony *[a]

Carbazole-based, π-conjugated donor–acceptor fluorophores were synthesized by integrating imidazole/thiazole units. Then, we investigated the impact of subtle structural changes on fluorescence properties. Carbazole integrated with imidazole (**Cz-I**) and carbazole integrated with thiazole (**Cz-T**) showed strong fluorescence in solution (quantum yield (Φ_f) = 0.18 (**Cz-I**) and 0.14 (**Cz-T**) compared with the standard quinine sulfate) and solid-state (Φ_f = 8.0% (**Cz-I**) and 14.6% (**Cz-T**)). **Cz-I** showed relatively more blue-shifted emission in solution compared with the solid-state (λ_{max} = 417 nm (CH_3CN) and 460 nm (solid)). **Cz-T** exhibited deep-blue emission in the solid-state compared with solution (λ_{max} = 455 nm (CH_3CN) and 418 nm (solid)). Interestingly, **Cz-T** exhibited a drastic change in fluorescence in organic solvents (CH_3CN, THF, CH_3OH, DMSO) with a low percentage (1%) of water. **Cz-I** showed reversible fluorescence switching between two fluorescence states upon exposure to trifluoracetic acid (TFA)/ammonia (NH_3). In contrast, **Cz-T** displayed reversible/self-reversible off–on fluorescence switching upon exposure to TFA or NH_3. Mechanofluorochromic studies of **Cz-I** showed a slight reduction in fluorescence intensity upon crushing and reversal to the initial state upon heating. **Cz-T** exhibited off–on reversible/self-reversible fluorescence switching upon crushing/heating. Computational studies indicated that thiazole integration improved the electron-withdrawing characteristics compared with imidazole and contributed to contrasting fluorescence responses. Thus, a simple change of nitrogen with sulfur produced contrasting self-assembly in the solid-state that led to different functional properties and stimuli-induced fluorescence switching.

Received 23rd March 2023
Accepted 10th April 2023

DOI: 10.1039/d3ra01897k

rsc.li/rsc-advances

Introduction

Organic molecules that emit fluorescence have been of great interest in recent decades because of their applications ranging from biological science to optoelectronic devices.[1–5] The molecular structure of a fluorophore, in general, plays an important part in fluorescence properties in solution and the solid-state.[6–9] For instance, planar polyaromatic molecules show strongly enhanced emission in solution and weak or no emission in the solid-state due to aggregation-induced quenching.[10,11] In contrast, fluorophores with a non-planar twisted structure often exhibit aggregation-induced emission/aggregation-induced enhanced emission (AIE/AIEE) in the solid-state compared with in solution.[12–14] Integrating a twisted non-planar group with a π-conjugated aromatic molecule has shown emission in solution as well as the solid-state.[15–17] Weak intermolecular interactions coupled with loose molecular packing in a twisted fluorophore produce stimuli-responsive fluorescence switching.[18–20] Stimuli-responsive fluorescence systems are potential materials for environmental/biosensing, information storage and anticounterfeiting.[21–25] A subtle structural change in a fluorophore is often employed to improve fluorescence efficiency as well as to achieve tunable and switchable fluorescence.[26–30] Control of molecular packing by substitution with an alkyl group can produce fluorescence gels, tunable solid-state fluorescence, room-temperature phosphorescence and different types of mechanofluorochromism.[31–37] Donor–acceptor structural "tailoring" can result in wide fluorescence tuning with improved fluorescence efficiency.[38–41] Halogen substitution with a fluorophore structure can significantly improve fluorescence efficiency and fluorescence switching by controlling the molecular organization.[42–44]

[a]*School of Chemical & Biotechnology, SASTRA Deemed University, Thanjavur 613401, Tamil Nadu, India. E-mail: philip@biotech.sastra.edu*

[b]*PG and Research Department of Chemistry, Khadir Mohideen College (Affiliated to Bharathidasan Univ.), Adirampattinam, Tamil Nadu, India*

[c]*Research Center for Advanced Materials Science, King Khalid University, Abha 61413, Saudi Arabia*

[d]*Department of Chemistry, King Khalid University, Abha 61413, Saudi Arabia*

[e]*Beamline Department, Pohang Accelerator Laboratory, 80 Jigokro-127 Beongil, Namgu, Pohang, Gyeongbuk, South Korea. E-mail: dmoon@postech.ac.kr*

† Electronic supplementary information (ESI) available: NMR, absorption, and emission spectra, PXRD and crystallographic figure. See DOI: https://doi.org/10.1039/d3ra01897k

Incorporating an acid-responsive functional group with a fluorophore allows fabrication of pH-controlled fluorescence-switching platforms.[45–47] Thus, exploring the role of structural change on the fluorescence properties of organic molecules is a highly active research field.

The rigid, planar, aromatic heterocyclic imidazole unit has been used as a building block for developing efficient fluorescence molecules with improved thermal stability and material attributes.[48–52] Herein, we synthesized a carbazole donor integrated with an imidazole (**Cz-I**) acceptor and thiazole (**Cz-T**) acceptor (Scheme 1) and explored the imidazole/thiazole effect on fluorescence properties. **Cz-I** and **Cz-T** showed emission in solution ($\Phi_f = 0.18$ (**Cz-I**) 0.14 (**Cz-T**) compared with a standard of quinine sulfate) and solid-state (8.0% (**Cz-I**) and 14.6% (**Cz-T**)). Interestingly, **Cz-T** showed deep-blue emission in the solid-state whereas **Cz-I** exhibited cyan emission. AIE studies of **Cz-I** and **Cz-T** revealed contrasting fluorescence changes upon aggregation from solution. Furthermore, **Cz-T** exhibited self-reversible mechanofluorochromism and halochromism compared with **Cz-I**. Hence, simple structural change by N/S produced contrasting fluorescence switching and fluorescence tuning.

Experimental

Carbazole, 4-bromobenzaldehyde, 18-crown-6, copper iodide, potassium carbonate, 2-aminothiophenol, *o*-phenylenediamine and solvents were procured from MilliporeSigma or Merck India, and used without further purification.

Synthesis of 4-(9*H*-carbazol-9-yl)benzaldehyde (Scheme S1†)

4-(9*H*-carbazol-9-yl)benzaldehyde was synthesized by a C–N coupling reaction between carbazole (1.8 g, 1 mmol) and 4-bromobenzaldhyde (2.38 g, 1.2 mmol) in the presence of K_2CO_3 (4.52 g, 3 mmol), CuI (0.26, 0.13 mmol) and 18-Crown-6 (0.08 g, 0.03 mmol) in *o*-dichlorobenzene (8 ml) at 180 °C for 24 h. The resultant mixture was extracted, concentrated, and purified by column chromatography to proffer a yield of 1.46 g (47%).

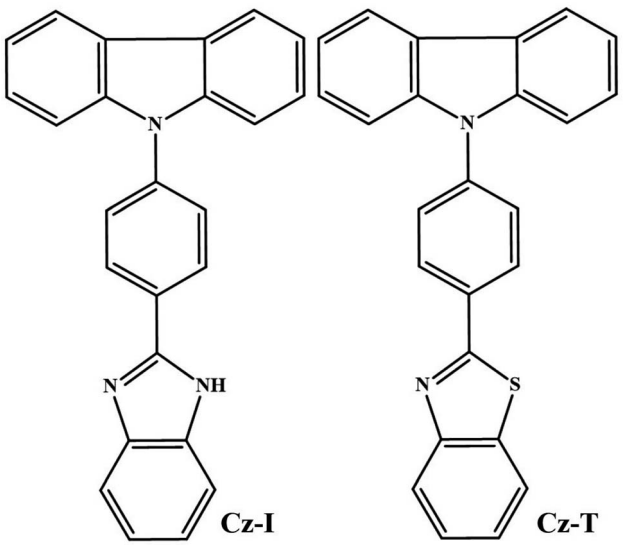

Scheme 1 Molecular structure of Cz-I and Cz-T.

Synthesis of 9-(4-(1*H*-benzo[*d*]imidazol-2-yl)phenyl)-9*H*-carbazole (Cz-I)

The aldehyde (0.5 g, 1 mmol) and *o*-phenylenediamine (0.08 g, 1 mmol) were mixed in acetic acid (2 ml) and refluxed for 5 h. After completion of the reaction, the reaction mixture was cooled and poured into cold water. The obtained precipitate was washed five-times with cold water, dried, and purified using column chromatography (EtOAc : Hexane (15 : 85) to proffer a yield of 0.529 g (80%)).

Synthesis of 2-(4-(9*H*-carbazol-9-yl)phenyl)benzo[*d*]thiazole (Cz-T)

The aldehyde (0.5 g, 1 mmol) and 2-aminothiophenol (0.08 g, 1 mmol) were dissolved in DMSO and refluxed at 120 °C for 8 h. After completion of the reaction, the reaction mixture was cooled and poured into cold water. The obtained precipitate was purified using column chromatography (EtOAc : Hexane (10 : 90)) to proffer a yield of 0.521 g (75%).

9-(4-(1*H*-benzo[*d*]imidazol-2-yl)phenyl)-9*H*-carbazole (Cz-I). M.p.: 270 °C. ^{1}H NMR (600 MHz, $CDCl_3$) δ 13.04 (s, 1H), 8.42–8.39 (d, 2H, $J = 12$ Hz), 8.24–8.21 (m, 2H, $J = 6$ Hz), 7.79–7.77 (d, 2H, $J = 12$ Hz), 7.65 (s, 1H), 7.53 (s, 1H), 7.46–7.40 (m, 4H, $J = 9$ Hz), 7.28–7.25 (t, 2H, $J = 6$ Hz), 7.20–7.17 (m, 2H, $J = 6$ Hz). ^{13}C NMR (150 MHz, $CDCl_3$) δ 151.03, 144.31, 140.33, 138.59, 135.58, 129.50, 128.66, 127.44, 126.89, 123.43, 123.26, 122.35, 121.07, 120.85, 119.46, 111.95, 110.29. *m/z* calculated $C_{25}H_{17}N_3$ (M + H): 359.14, found: 359.2.

2-(4-(9*H*-carbazol-9-yl)phenyl)benzo[*d*]thiazole (Cz-T). M.p.: 191 °C. ^{1}H NMR (600 MHz, $CDCl_3$) δ 8.20–8.18 (d, 2H, $J = 12$ Hz), 8.05–7.96 (m, 3H, $J = 7$ Hz), 7.82–7.81 (d, 1H, $J = 6$ Hz), 7.59–7.58 (d, 2H, $J = 6$ Hz), 7.42–7.38 (m, 2H, $J = 9$ Hz), 7.34–7.25 (m, 3H, $J = 6$ Hz), 7.22–7.20 (m, 2H, $J = 6$ Hz), 7.13–7.10 (m, 1H, $J = 9$ Hz). ^{13}C NMR (150 MHz, $CDCl_3$) δ 167.07, 154.31, 140.55, 140.27, 139.62, 135.29, 132.43, 129.18, 127.32, 126.67, 126.30, 125.92, 125.56, 123.84, 123.48, 121.86, 120.57, 120.43, 119.51, 110.71, 109.95. *m/z* calculated $C_{25}H_{16}N_2S$ (M + H): 376.14, found: 376.2.

Characterization

Nuclear magnetic resonance (NMR) spectroscopy was done on a 600 MHz system from JEOL. Fluorescence spectra and the absolute quantum yield for all compounds in the solid-state were recorded using a fluorescence spectrometer (FP-8300; Jasco) equipped with an integrating sphere and calibrated light source. Absorption spectroscopy was done on a UV-visible spectrophotometer (V-730ST; Jasco). A triple quadrupole mass spectrometer (6475 series; Agilent Technologies) was used to obtain mass. Powder X-ray diffraction (PXRD) patterns were measured using a X-ray diffractometer (D8 Advance; Bruker) with Cu Kα radiation (λ = 1.54050 Å) at room temperature. Single crystals were coated with paratone-N oil and diffraction data measured with synchrotron radiation (λ = 0.62998 Å) on

a ADSC Quantum-210 detector at 2D SMC with a silicon (111) double-crystal monochromator at the Pohang Accelerator Laboratory, Korea. The highest occupied molecular orbital (HOMO), lowest occupied molecular orbital (LUMO) and bandgap of all structures were studied using B3PW91/6-31 + G(d,p) level theory (Gaussian 09 package).

Results and discussion

Cz-I and **Cz-T** were synthesized as shown in Scheme 1. The absorption spectra of **Cz-I** and **Cz-T** showed an intramolecular charge transfer (ICT) band between 330 nm and 340 nm (Fig. S1†). Furthermore, the solvent polarity did not show a significant effect on absorption, thereby indicating the non-polar ground state of both molecules. In contrast, both molecules exhibited solvent polarity-dependent fluorescence tuning between 384 nm and 424 nm for **Cz-I** and between 413 nm and 470 nm for **Cz-T** (Fig. 1 and Table 1). **Cz-I** in $CHCl_3$ showed weak broad fluorescence between 375 nm and 480 nm (Fig. 1a). Furthermore, **Cz-I** showed strong fluorescence in non-polar and polar aprotic solvents, whereas **Cz-T** exhibited strong fluorescence in non-polar solvents and weak fluorescence in polar solvents. **Cz-I** showed relatively blue-shifted fluorescence compared with **Cz-T**, which showed gradual red-shifting of fluorescence upon increasing the solvent polarity. These fluorescence changes across changes in solvent polarity indicated that sulfur in thiazole groups increased their electron-withdrawing character and produced ICT from the carbazole donor to the thiazole acceptor. However, nitrogen in an imidazole compound might interfere with the ICT from carbazole to imidazole due to the electron-donating characteristics of nitrogen. Computational studies (see below) also suggested a ICT in **Cz-T** compared with **Cz-I**. Interestingly, **Cz-T** showed weak excimeric emissions at longer wavelengths (between 680 nm and 715 nm as well as 829 nm) (Fig. 1b). Concentration-dependent studies of **Cz-T** in EtOAc clearly exhibited an increase in excimer emission intensity at higher concentrations (Fig. 1c). In contrast, **Cz-I** did not show any excimeric emission.

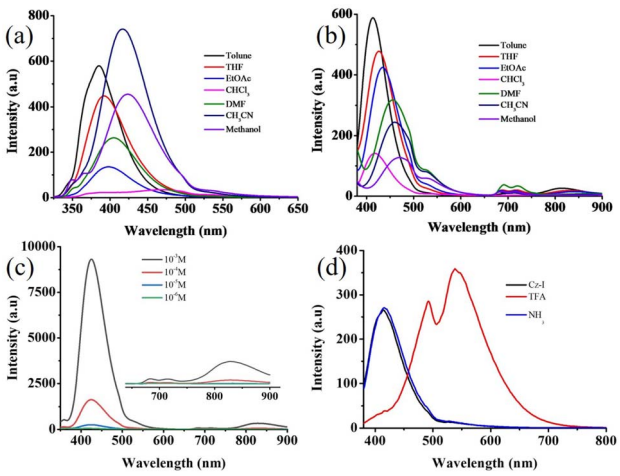

Fig. 1 Fluorescence spectra of (a) **Cz-I** and (b) **Cz-T** in different solvents. (c) Concentration-dependent fluorescence spectra of **Cz-T** in EtOAc. (d) Acid/base-dependent fluorescence switching of **Cz-I** in CH_3CN. λ_{exc} = 320 nm.

Table 1 Fluorescence λ_{max} and quantum of yield (Φ_f) of **Cz-I** and **Cz-T** in different solvents. Quantum yield was measured by comparison with a standard (0.5 M quinine sulfate)

	Cz-I		**Cz-T**	
Solvent	λ_{max} (nm)	Φ_f	λ_{max} (nm)	Φ_f
Toluene	384	0.18	413	0.14
THF	391	0.11	431	0.13
EtOAc	397	0.04	436	0.08
$CHCl_3$	375–480 (weak broad)	—	416	0.03
DMF	405	0.08	457	0.09
CH_3CN	417	0.17	455	0.05
MeOH	424	0.09	470	0.03

The presence of nitrogen in **Cz-I** and **Cz-T** along with good fluorescence was expected to show a response towards pH. **Cz-I** showed red-shifting of fluorescence from 417 nm to 538 nm upon addition of trifluoroacetic acid (TFA) in CH_3CN (Fig. 1d). Ammonia addition exhibited perfect reversibility of emission to the initial state. A slow increase in the TFA concentration showed a gradual decrease of emission at 417 nm and emergence of a new peak at 538 nm (Fig. 2a). Similarly, an increase in the ammonia concentration led to a gradual decrease of longer-wavelength emission at 538 nm and reappearance of shorter-wavelength emission at 417 nm (Fig. 2b). TFA addition and ammonia addition showed an isosbestic point, and suggested a dynamic equilibrium between the protonated species and non-protonated species in the solution. Along with strong emission at 538 nm in an acidic medium, a "hump" was noted at 490 nm. Thus, **Cz-I** showed reversible fluorescence switching between two emissive states upon addition of TFA and ammonia. The gradual reduction of emission at 417 nm along with emergence of emission at 538 led to dual emission with an increasing TFA concentration. This phenomenon allowed control of dual emission by adjusting the acid concentration and produced white emission (Fig. 2c). **Cz-I** also exhibited fluorescence tuning as well as white emission upon addition of acetic acid and *para*-toluene sulphonic acid (Fig. 2c). In contrast, addition of TFA into a CH_3CN solution of **Cz-T** showed complete quenching of fluorescence (Fig. S2†). Surprisingly, it did not show reversible "turn on" fluorescence upon ammonia addition, and remained in the quenched state.

Cz-I and **Cz-T** showed strong solid-state fluorescence due to integration of a twisted *N*-phenyl carbazole unit with imidazole/thiazole (Fig. 3a). **Cz-T** showed deep-blue emission (λ_{max} = 418 nm, Φ_f = 14.6%) whereas is **Cz-I** showed cyan emission (λ_{max} = 460 nm, Φ_f = 8.0%). Interestingly, compared with the solution state, the emission peak was blue-shifted for **Cz-T** in the solid-state but red-shifted for **Cz-I**. AIE studies in a CH_3CN–water mixture confirmed the opposite shift of fluorescence upon moving from solution to an aggregated state (Fig. 3b and c). **Cz-I** in CH_3CN showed strong fluorescence at 417 nm. It

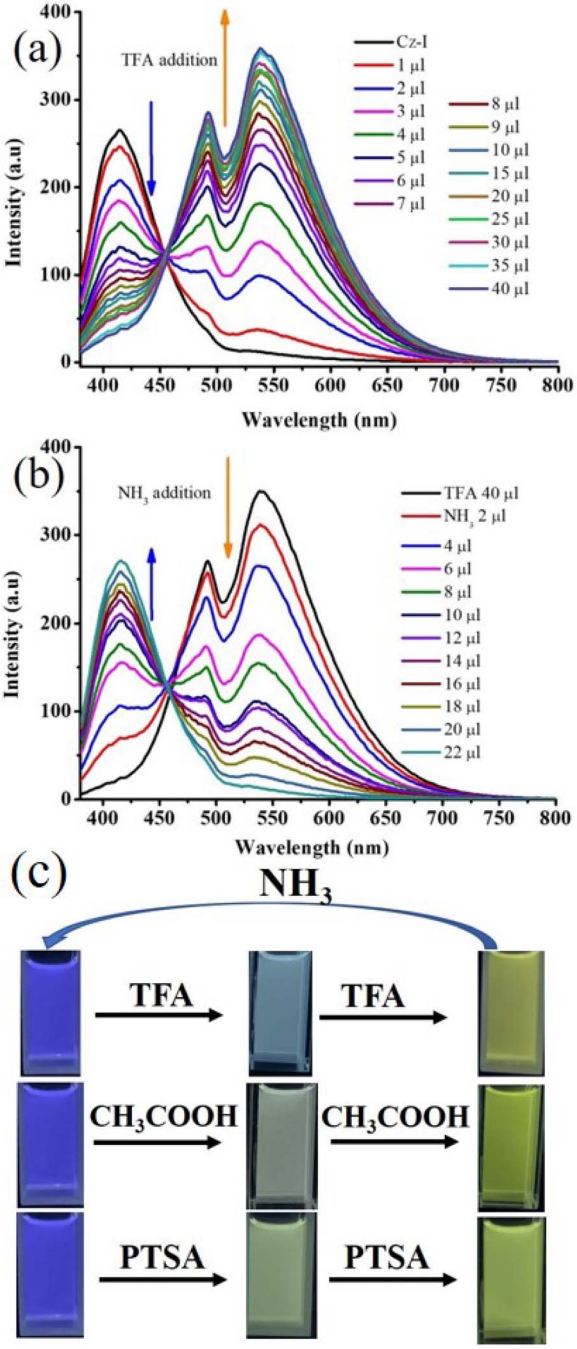

Fig. 2 Halochromic reversible fluorescence switching of **Cz-I**. (a) Addition of TFA (10^{-3} M) into **Cz-I**. (b) NH_3 (10^{-3} M) addition into **Cz-I** + TFA in CH_3CN. (c) Digital fluorescence images of **Cz-I** with different acids. λ_{exc} = 320 nm (spectra) and 365 nm (digital images).

showed a red-shift of the emission peak (λ_{max} = 424 nm) in a 10% water–CH_3CN mixture (Fig. 3b). Further increases in the water fraction showed only a slight red-shift with reduction of fluorescence intensity. However, the fluorescence intensity was strongly reduced with broad red-shifted emission at >80% water fraction. **Cz-T** exhibited strong fluorescence at 455 nm in CH_3CN. An increase in the water fraction to 10% led to red-shift of emission to 470 nm with a drastic change in emission colour.

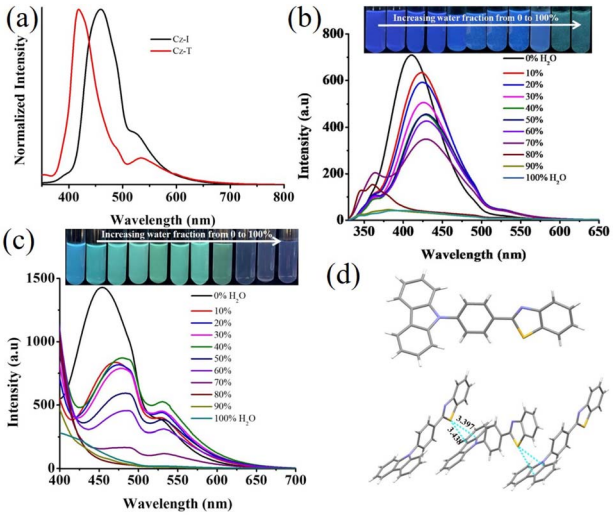

Fig. 3 (a) Solid-state fluorescence spectra of **Cz-I** and **Cz-T**. AIE studies of (b) **Cz-I** and (c) **Cz-T** in a CH_3CN–water mixture and molecular structure and (d) intermolecular interactions in the crystal lattice of **Cz-T**. C (gray), H (white), N (blue) and S (yellow). The dotted lines indicate the intermolecular distance in Å. λ_{exc} = 320 (spectra) and 365 nm (digital images).

Further increases in the water fraction (up to 60%) showed a reduction of fluorescence intensity. The emission peak at 455 nm disappeared completely at >70% water fraction and showed blue-shifted emission. The drastic change in **Cz-T** fluorescence with increasing water content in CH_3CN suggested possible utility as a fluorescent water sensor in solvents. To confirm the water-sensing characteristics of **Cz-T**, water-miscible solvents (CH_3CN, DMSO, DMF, THF) were chosen and we monitored the change in fluorescence with increasing water percentage from 1% upwards (Fig. S3†). Interestingly, all four solvents showed a fluorescence change upon addition of 1% water and also exhibited a linear change with increasing water percentage up to 10%.

The opposite change in fluorescence from solution to an aggregated state indicated that both compounds might adopt different molecular arrangements in the solid-state. However, only **Cz-T** produced crystals of sufficient quality for structural analyses. The structural parameters of **Cz-T** matched perfectly with a structure reported previously.[53] The thiazole group and phenyl group attached with thiazole adopted a coplanar conformation, but displayed a twisted conformation with a carbazole unit (Fig. 3d). The twisted molecular structure hindered the π···π stacking in the crystal lattice (Fig. S4†). The sulfur atom involved in the S···π interaction with the carbazole unit rigidified the molecule in the solid-state (Fig. 3d). The sulfur intermolecular interaction and opposite molecular arrangement might have contributed to deep-blue emission. To understand the electronic transition, computational studies were undertaken using the B3PW91/6-31G(d,p) level of theory for **Cz-I** and **Cz-T**. The structure of **Cz-T** was chosen from the single-crystal structure and used without structural optimization. However, a geometry-optimized structure was used for **Cz-I**

because it did not produce single crystals. The (HOMO) of **Cz-I** indicated electron density in the whole structure, and movement from carbazole to phenyl-imidazole units in the LUMO (Fig. 4). In contrast, electron density was occupied mostly in the carbazole-phenyl unit in the HOMO and shifted to the phenyl-thiazole unit in the LUMO of **Cz-T**. Thus, **Cz-T** exhibited an electronic transition from a carbazole donor to a thiazole acceptor, and supported ICT (Fig. 4).

The good solid-state fluorescence with a twisted molecular structure along with acid-responsive nitrogen suggested the possibility of obtaining stimuli-responsive fluorescence switching. The crushing of **Cz-I** showed reduction of fluorescence intensity with slight blue-shifting of λ_{max} (Fig. 5a). Fluorescence was reversed to the initial state by heating. In contrast, **Cz-T** exhibited complete reduction of fluorescence intensity by crushing (Fig. 5c). Fluorescence was reversed to the initial state by heating. **Cz-T** showed slight blue-shifted emission (404 nm) after heating that could be attributed to the crystal habits.[48,54,55] **Cz-T** also exhibited self-reversible fluorescence switching from the crushing state without the need for heating (Fig. 6a). After 4 h, it showed significant enhancement of fluorescence intensity and self-reversed completely to the initial state in 24 h. Conversely, the fluorescence intensity of crushed **Cz-I** was reduced further with time without altering the peak position (Fig. 6b). After 24 h, it showed shifting of emission peak position to the initial state. Though the peak position of **Cz-I** self-reversed to the initial state, its intensity remained reduced without heating. TFA exposure to **Cz-I** solids led to an increase in fluorescence intensity with red-shifting of the emission peak from 460 nm to 483 nm (Fig. 5b). Fluorescence was reversed to the initial state by NH_3 exposure. In contrast, fluorescence was reduced significantly with red-shifting of the peak position by TFA exposure to **Cz-T** (Fig. 5d). Fluorescence was reversed completely to the initial state by NH_3 exposure. As observed in mechanofluorochromism, **Cz-T** also showed self-reversible fluorescence switching after TFA exposure with time (Fig. 6c), but **Cz-I** did not show self-reversibility. Thus, **Cz-I** exhibited fluorescence switching between two fluorescence states by TFA/NH_3 exposure, but **Cz-T** exhibited off–on reversible/self-reversible fluorescence switching. **Cz-T** did not show reversible fluorescence switching by acid/base exposure in solution. In general, fluorescence tuning by crushing can be attributed to transformation of the crystalline phase to amorphous/partial amorphous state.[56–61] The molecular planarization and close stacking caused reduction of fluorescence intensity. The conversion of the amorphous/partial amorphous phase to the crystalline state by heating induced reversible fluorescence switching. PXRD studies were performed to confirm the reversible phase transformation for **Cz-I** and **Cz-T** (Fig. 6d). Initial samples showed sharp diffraction peaks and indicated crystallinity before crushing. Crushed samples also showed sharp diffraction peaks even without heating because the compounds exhibited self-reversibility with time. The perfect matching of diffraction peaks before and after crushing/heating

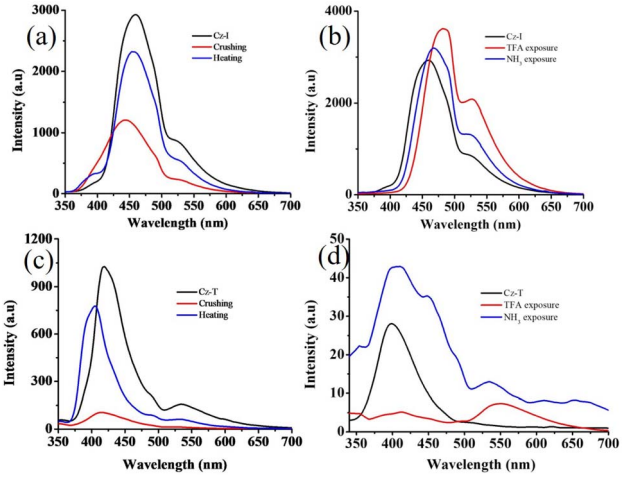

Fig. 5 (a and c) Reversible fluorescence switching of (a and b) **Cz-I** and (c and d) **Cz-T** by (a and c) crushing/heating and (b and d) TFA/NH_3 exposure. λ_{exc} = 320 nm.

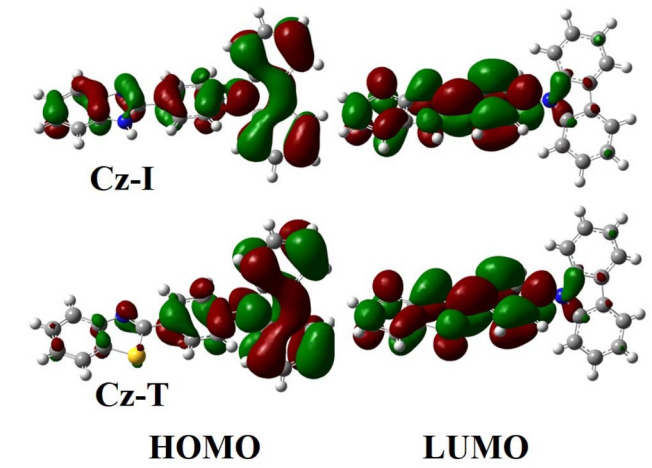

Fig. 4 HOMO–LUMO diagrams for **Cz-I** and **Cz-T**.

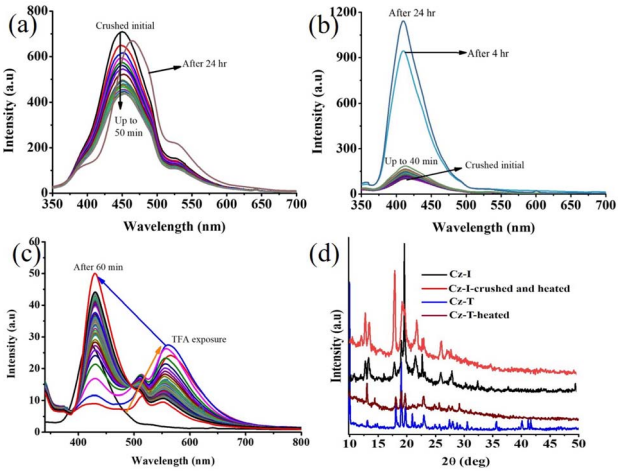

Fig. 6 Self-reversible fluorescence switching of (a) **Cz-I** and (b and c) **Cz-T** by (a and b) crushing and (b) TFA exposure. (d) PXRD patterns of pristine and crushed samples. λ_{exc} = 320 nm.

suggested an absence of chemical transformation upon crushing/heating. Thus, simple replacement of imidazole by thiazole in the donor–acceptor compound produced contrasting fluorescence properties that could be attributed to the electronic characteristics of the sulfur atom.

Conclusions

A carbazole π-conjugated fluorophore with imidazole/thiazole acceptor units was synthesized and demonstrated contrasting fluorescence properties by subtle structural changes. The fluorophore with imidazole (**Cz-I**) and thiazole (**Cz-T**) showed different fluorescence intensity in solution and the solid-state. **Cz-I** showed deep-blue emission (λ_{max} = 417 nm) in solution whereas **Cz-T** exhibited red-shifted emission (λ_{max} = 455 nm). In the aggregated state, **Cz-I** showed red-shifted emission (λ_{max} = 460 nm) and **Cz-T** showed deep-blue emission (λ_{max} = 418 nm). HOMO–LUMO theoretical calculation suggested ICT in **Cz-T** compared with **Cz-I**, and this could be attributed to the difference in electronic characteristics between N and S. Single-crystal analyses of **Cz-T** showed that S···π interactions facilitated opposite molecular arrangements in the crystal lattice and contributed to deep-blue emission in the solid-state. Interestingly, **Cz-T** exhibited reversible/self-reversible off–on fluorescence switching upon crushing/heating and exposure to TFA/NH_3. **Cz-I** showed reversible fluorescence switching between two fluorescence states upon crushing/heating and TFA/NH_3 exposure. Thus, a carbazole-imidazole fluorophore exhibited contrasting fluorescence switching and fluorescence tuning upon subtle structural changes.

Conflicts of interest

There are no conflicts to declare.

Acknowledgements

Financial support from the Science and Engineering Research Board (SERB), Core Research Grant (CRG/2020/003978) and DST-FIST (SR/FST/CS-1/2018/62), New Delhi, India, is acknowledged with gratitude. The Deanship of Scientific Research at King Khalid University (R.G.P.1/274/43) is greatly appreciated. Studies on X-ray crystallography were supported by Basic Science Research Program through the National Research Foundation of Korea funded by the Ministry of Education, Science and Technology (NRF-2021R1A2C1003080).

References

1 Z. Chi, X. Zhang, B. Xu, X. Zhou, C. Ma, Y. Zhang, S. Liu and J. Xu, *Chem. Soc. Rev.*, 2012, **41**, 3878.
2 Y. Wang, Y. Liao, C. P. Cabry, D. Zhou, G. Xie, Z. Qu, D. W. Bruce and W. Zhu, *J. Mater. Chem. C*, 2017, **5**, 3999–4008.
3 J. Zhang, B. Xu, J. Chen, S. Ma, Y. Dong, L. Wang, B. Li, L. Ye and W. Tian, *Adv. Mater.*, 2014, **26**, 739–745.
4 S. Suzuki, S. Sasaki, A. S. Sairi, R. Iwai, B. Z. Tang and G. Konishi, *Angew. Chem. Int. Ed.*, 2020, **59**, 9856–9867.
5 C. Wang, Y. Yu, Y. Yuan, C. Ren, Q. Liao, J. Wang, Z. Chai, Q. Li and Z. Li, *Matter*, 2020, **2**, 181–193.
6 S. P. Anthony, *Chempluschem*, 2012, **77**, 518–531.
7 J. Gierschner, J. Shi, B. Milián-Medina, D. Roca-Sanjuán, S. Varghese and S. Park, *Adv. Opt. Mater.*, 2021, **9**, 2002251.
8 H.-Y. Fu, X.-J. Liu and M. Xia, *RSC Adv.*, 2017, **7**, 50720–50728.
9 L. Huang, Y. Qiu, C. Wu, Z. Ma, Z. Shen and X. Jia, *J. Mater. Chem. C*, 2018, **6**, 10250–10255.
10 Z. Zhao, S. Chen, J. W. Y. Lam, Z. Wang, P. Lu, F. Mahtab, H. H. Y. Sung, I. D. Williams, Y. Ma, H. S. Kwok and B. Z. Tang, *J. Mater. Chem.*, 2011, **21**, 7210.
11 A. C. Grimsdale, K. Leok Chan, R. E. Martin, P. G. Jokisz and A. B. Holmes, *Chem. Rev.*, 2009, **109**, 897–1091.
12 G. R. Suman, M. Pandey and A. S. J. Chakravarthy, *Mater. Chem. Front.*, 2021, **5**, 1541–1584.
13 X. Lou and Y. Yang, *Aggregate*, 2020, **1**, 19–30.
14 D. Wang, M. M. S. Lee, W. Xu, G. Shan, X. Zheng, R. T. K. Kwok, J. W. Y. Lam, X. Hu and B. Z. Tang, *Angew. Chem. Int. Ed.*, 2019, **58**, 5628–5632.
15 J. L. Belmonte-Vázquez, Y. A. Amador-Sánchez, L. A. Rodríguez-Cortés and B. Rodríguez-Molina, *Chem. Mater.*, 2021, **33**, 7160–7184.
16 F. Yu, H. Zhao, Y. Li, G. Xia and H. Wang, *Mater. Chem. Front.*, 2022, **6**, 155–162.
17 A. Kundu, S. Karthikeyan, D. Moon and S. P. Anthony, *J. Fluoresc.*, 2019, **29**, 1359–1369.
18 C. Wang and Z. Li, *Mater. Chem. Front.*, 2017, **1**, 2174–2194.
19 S. Ito, *Chem. Lett.*, 2021, **50**, 649–660.
20 Z. Yang, Z. Chi, Z. Mao, Y. Zhang, S. Liu, J. Zhao, M. P. Aldred and Z. Chi, *Mater. Chem. Front.*, 2018, **2**, 861–890.
21 P. Gayathri, S. Ravi, P. Nantheeswaran, M. Mariappan, S. Karthikeyan, M. Pannipara, A. G. Al-Sehemi, D. Moon and S. P. Anthony, *Mol. Syst. Des. Eng.*, 2022, **7**, 1277–1286.
22 P. S. Hariharan, E. M. Mothi, D. Moon and S. P. Anthony, *ACS Appl. Mater. Interfaces*, 2016, **8**, 33034–33042.
23 Y. Ma, Y. Yu, J. Li, S. Liu, W. Huang and Q. Zhao, *InfoMat*, 2021, **3**, 82–100.
24 H. Jia, Y. Teng, N. Li, D. Li, Y. Dong, D. Zhang, Z. Liu, D. Zhao, X. Guo, W. Di and W. Qin, *ACS Mater. Lett.*, 2022, **4**, 1306–1313.
25 Y. Zhuang, X. Ren, X. Che, S. Liu, W. Huang and Q. Zhao, *Adv. photonics*, 2021, **3**, 014001.
26 F. Khan, M. Mahmoudi, D. Volyniuk, J. V. Grazulevicius and R. Misra, *J. Phys. Chem. C*, 2022, **126**, 15573–15586.
27 Q. Li, S. Li, K. Wang, Y. Zhou, Z. Quan, Y. Meng, Y. Ma and B. Zou, *J. Phys. Chem. C*, 2017, **121**, 1870–1875.
28 H.-Q. Peng, X. Zheng, T. Han, R. T. K. Kwok, J. W. Y. Lam, X. Huang and B. Z. Tang, *J. Am. Chem. Soc.*, 2017, **139**, 10150–10156.
29 M. Fang, J. Yang, Q. Liao, Y. Gong, Z. Xie, Z. Chi, Q. Peng, Q. Li and Z. Li, *J. Mater. Chem. C*, 2017, **5**, 9879–9885.
30 P. Gayathri, S. Karthikeyan, M. Pannipara, A. G. Al-Sehemi, D. Moon and S. P. Anthony, *Cryst. Growth Des.*, 2022, **22**, 5432–5440.

31 Y. Yu, Y. Fan, C. Wang, Y. Wei, Q. Liao, Q. Li and Z. Li, *Mater. Chem. Front.*, 2021, **5**, 817–824.
32 P. S. Hariharan, D. Moon and S. P. Anthony, *CrystEngComm*, 2017, **19**, 6489–6497.
33 Q. Huang, X. Mei, Z. Xie, D. Wu, S. Yang, W. Gong, Z. Chi, Z. Lin and Q. Ling, *J. Mater. Chem. C*, 2019, **7**, 2530–2534.
34 W. Li, Q. Huang, Z. Mao, Q. Li, L. Jiang, Z. Xie, R. Xu, Z. Yang, J. Zhao, T. Yu, Y. Zhang, M. P. Aldred and Z. Chi, *Angew. Chem. Int. Ed.*, 2018, **57**, 12727–12732.
35 Y. Xie, Y. Ge, Q. Peng, C. Li, Q. Li and Z. Li, *Adv. Mater.*, 2017, **29**, 1606829.
36 Y. Wen, H. Liu, S. Zhang, J. Cao, J. De and B. Yang, *Adv. Opt. Mater.*, 2020, **8**, 1901995.
37 P. S. Hariharan, P. Gayathri, D. Moon and S. P. Anthony, *ChemistrySelect*, 2017, **2**, 7799–7807.
38 Y. Zuo, J. Liu, P. Li, K. Li, J. W. Y. Lam, D. Wu and B. Z. Tang, *Cell Rep. Phys. Sci.*, 2023, **4**, 101202.
39 P. Gayathri, S. B. Subramaniyan, A. Veerappan, M. Pannipara, A. G. Al-Sehemi, D. Moon and S. P. Anthony, *Cryst. Growth Des.*, 2022, **22**, 633–642.
40 P. S. Hariharan, V. K. Prasad, S. Nandi, A. Anoop, D. Moon and S. P. Anthony, *Cryst. Growth Des.*, 2017, **17**, 146–155.
41 P. S. Hariharan, G. Parthasarathy, A. Kundu, S. Karthikeyan, Y. Sagara, D. Moon and S. P. Anthony, *Cryst. Growth Des.*, 2018, **18**, 3971–3979.
42 H. Li, H. Shu, Y. Liu, X. Wu, H. Tian, H. Tong and L. Wang, *Adv. Opt. Mater.*, 2019, **7**, 1801719.
43 Z. Zhou, Q. Liu, X. Chen, G. Xu, S. Wang, Y. Tu, J. Zhang, X. Zheng, J. Xiang, X. Feng, Y. Zhang, S. Xie, Z. Zeng and B. Z. Tang, *Adv. Funct. Mater.*, 2021, **31**, 2009024.
44 A. D'Aléo, A. Saul, C. Attaccalite and F. Fages, *Mater. Chem. Front.*, 2019, **3**, 86–92.
45 P. Gayathri, M. Pannipara, A. G. Al-Sehemi, D. Moon and S. P. Anthony, *Mater. Adv.*, 2021, **2**, 996–1005.
46 P. Gayathri, P. Nag, N. Anand, S. R. Vennapusa, M. Pannipara, A. G. Al-Sehemi, D. Moon and S. P. Anthony, *New J. Chem.*, 2021, **45**, 22450–22460.
47 T. Sachdeva and M. D. Milton, *Dyes Pigm.*, 2019, **164**, 305–318.
48 H.-Y. Fu, X.-J. Liu, H. Zha, X.-X. Li, Y. Xu, F. Yang and M. Xia, *Phys. Chem. Chem. Phys.*, 2019, **21**, 1399–1407.
49 J. Liu, J. Chen, Y. Dong, Y. Yu, S. Zhang, J. Wang, Q. Song, W. Li and C. Zhang, *Mater. Chem. Front.*, 2020, **4**, 1411–1420.
50 S. Petdee, C. Chaiwai, W. Benchaphanthawee, P. Nalaoh, N. Kungwan, S. Namuangruk, T. Sudyoadsuk and V. Promarak, *Dyes Pigm.*, 2021, **193**, 109488.
51 W.-C. Chen, Y. Yuan, G.-F. Wu, H.-X. Wei, L. Tang, Q.-X. Tong, F.-L. Wong and C.-S. Lee, *Adv. Opt. Mater.*, 2014, **2**, 626–631.
52 J. Tagare, H. Ulla, M. N. Satyanarayan and S. Vaidyanathan, *J. Lumin.*, 2018, **194**, 600–609.
53 Y. Gong, *CCDC 1952420: Experimental Crystal Struct. Determination*, 2019, DOI: **10.5517/ccdc.csd.cc23jn9m**.
54 L. Zou, S. Guo, H. Lv, F. Chen, L. Wei, Y. Gong, Y. Liu and C. Wei, *Dyes Pigm.*, 2022, **198**, 109958.
55 X. Zhang, Y. Liu, W. Wei, L. Gao, Y. Duan, H. Han and T. Han, *Dyes Pigm.*, 2022, **197**, 109916.
56 P. S. Hariharan, D. Moon and S. P. Anthony, *J. Mater. Chem. C*, 2015, **3**, 8381–8388.
57 P. Sudhakar and T. P. Radhakrishnan, *J. Mater. Chem. C*, 2019, **7**, 7083–7089.
58 A. Kundu, P. S. Hariharan, K. Prabakaran, D. Moon and S. P. Anthony, *RSC Adv.*, 2015, **5**, 98618–98625.
59 Y. Zhan, Q. Wei, J. Zhao and X. Zhang, *RSC Adv.*, 2017, **7**, 48777–48784.
60 F. Qi, J. Lin, X. Wang, P. Cui, H. Yan, S. Gong, C. Ma, Z. Liu and W. Huang, *Dalton Trans.*, 2016, **45**, 7278–7284.
61 T. T. Divya, K. Ramshad, V. C. Saheer and L. Chakkumkumarath, *New J. Chem.*, 2018, **42**, 20227–20238.